Lasers in Manufacturing Conference 2019

Selective Multibeam micro processing of metal with a 1x8 beam array

Alexander Meyer[a]*, Johannes Finger[a], Oliver Nottrodt[a], Michael Jüngst[a]

[a]*Fraunhofer Institute for Laser Technology ILT, Steinbachstr. 15, 52074 Aachen, Germany*

Abstract

Processing metals by means of ultrashort pulsed laser radiation with pulse durations below approx. 12 ps yields higher surface quality, higher precision and smaller thermal stress compared to processing with pulsed laser radiation of longer pulse duration. To increase the productivity and use the available laser power efficiently, an approach for parallelization of the processing using a flexible multibeam setup is presented. The laser beam is split into 8 beamlets by a Diffractive Optical Element (DOE). All beams are moved across the workpiece using a high speed galvanometer scanner in combination with an f-theta lens. Each beam is individually switchable by means of an acousto-optic modulator (AOM) enabling multibeam bitmap structuring. Real-time control of the multi-channel modulator is realized with an FPGA and a time-based control scheme. Grey-scale information of the bitmaps is used as layer information, enabling the generation of arbitrary 2.5D surface structures. A threefold decrease in processing time is achieved.

Keywords: Multibeam; ultrafast; parallel processing; micro processing

1. Introduction

Ultrafast lasers in the picosecond (ps) range provide excellent machining quality for a broad range of materials, including ceramics, metals, and dielectrics. High quality microstructures in the micrometer range are possible, in combination with a very low thermal load on the material and no melt or recast. However, to achieve this high quality, the applied laser fluence needs to be in a narrow window around an optimal fluence which is typically about seven times (Raciukaitis 2009) the threshold fluence for ablation of the processed material. In combination with a small laser focus diameter to achieve small feature sizes, less than

Corresponding author. Tel.: +49 241 8906-8189; fax: +49 241 8906-121.
E-mail address: alexander.meyer@ilt.fraunhofer.de

10 W of laser power can be applied to a workpiece with a single spot approach and conventional galvanometer scanner systems.

For the processing of large surfaces like embossing tools in the range of a square meter, a single spot process is very time consuming and therefore not applicable from an economic point of view in many cases.

The availability and cost of industrial grade high power USP lasers have for a long time prevented the upscaling of USP processes to macro applications in the industrial context. However, this problem has been solved over the last years. Today, reliable high power USP lasers with up to 250 W of average output power are available (Edgewave GmbH 2019; AMPHOS GmbH 2019; Du et al. 2012; Russbueldt et al. 2010) at reasonable costs. Now, the challenge is to efficiently apply the available power for laser materials processing. In this work, we chose a switchable multibeam optics to divide the beam into multiple beamlets and thus distribute the available laser power across the workpiece. For static, non-switchable setups, this approach is already well known and allows for significant increase of productivity for processes such as the drilling of periodic hole patterns for filter applications (Gillner et al. 2015). Our approach addresses the limitation to periodic structures by including independent switching of every beamlet by means of an AOM and thus enables the parallel processing of arbitrary structures.

2. Experimental setup

The experimental setup as shown in Figure 1 is a scanner based optical approach that can be attached to every standard machining center. Since laser, scanner and AOMs need to operate in a synchronized manner, the software for data pre-processing and process control is a key component. The following paragraphs outline the hardware used, the implemented control schematic and the data preparation to process a bitmap image to the required scanner and AOM commands.

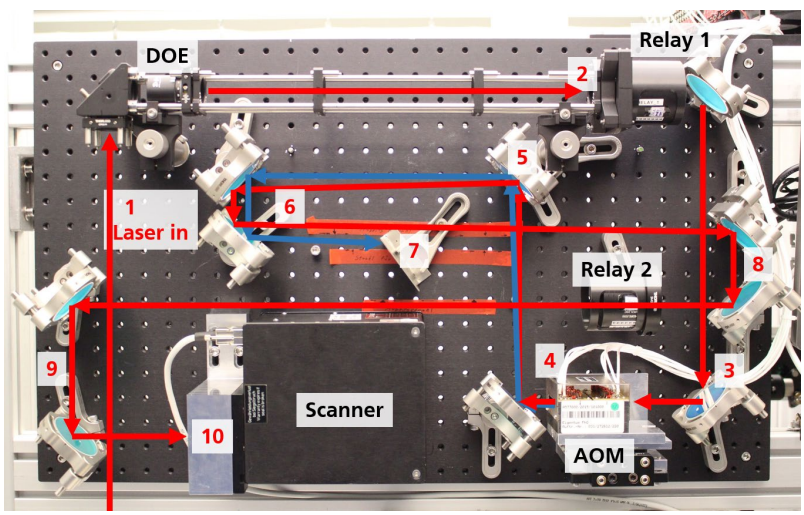

Fig. 1. Experimental Setup in an open lab configuration. The numbers indicate the order of elements within the folded beam path. Special positions are:
1 : Input of the beam into the optics, starting with the DOE.
4 : After passing the AOM, the beam is split into the diffracted « working beamlets » (red) and the non-diffracted zero-order-beampath (blue).
7 : The zero-order-beampath is guided into the beam dump.

2.1. Hardware

The laser source is a 10 ps laser manufactured by EdgeWave with a wavelength of 1064 nm. The maximum output power is 100 W, the repetition rate can be set in a range between 400 kHz and 20 MHz.

The DOE is manufactured by TOPAG Lasertechnik GmbH with a separation angle between neighboring beamlets of 0.449° and an efficiency of approx. 67 % with respect to the incoming intensity.

The Multi-Channel-AOM is manufactured by Gooch & Housego and made of tellurium dioxide. The pitch between the channels for neighboring beamlets is 4 mm. The AOM is controlled by a multifunction reconfigurable I/O device by National Instruments that features a Virtex 5 FPGA and a specially designed interface electronics.

The scanner is an IntelliScan manufactured by Scanlab, controlled by a RTC5 Scanner card. The focusing optics is a f-theta lens with 100 mm focal length is used.

The desired pitch between neighboring beamlets on the workpiece is 400 µm. Thus, a 10:1 projection between AOM (4 mm pitch) and workpiece is necessary. Combining a 4f setup with the aforementioned f-theta optics, this results in a beampath of approx. 4 m in length, which is folded multiple times to realize a compact setup (see Figure 1).

2.2. Efficiency & Calibration

In contrast to single spot processing, a significant amount of the laser power cannot be used for processing of the workpiece. Both the DOE and the AOM have an efficiency of approx. 67 %, which implies an overall efficiency limit of 45 % for the optical setup.

Furthermore, neither the DOE nor the AOM are perfectly homogeneous. Combined, the two inhomogeneities cause a difference in laser power of up to 11 % between the weakest and strongest beamlet. This is compensated by adjusting the RF power separately for each AOM channel to match all channels to the weakest one. Table 1 lists the result of this calibration. The overall efficiency of the optical system is reduced to 41 % by this measure.

Overall, the optical system reduces the applicable laser average output power to 43 W, equally splitted into eight beamlets with 5.4 W each.

Table 1: Calibration of the AOM channels. The RF power for each channel is adjusted to match all channels to the weakest ones (channels 1 and 8). Laser output power is 10.7 W before the optical system.

Beamlet / AOM Channel	Output Power[W] uncalibrated	Calibration Factor w.r.t. max RF Power	Output Power [W] calibrated
1	0.56	1	0.57
2	0.60	0.806	0.57
3	0.63	0.778	0.57
4	0.60	0.813	0.57
5	0.60	0.911	0.57
6	0.62	0.813	0.57
7	0.60	0.973	0.57
8	0.56	1	0.56

2.3. Process schematics

The schematic of the processing is shown in Figure 2. The control software creates an ablation job based on a grayscale bitmap file. The scanner moves the beam array in x direction across the workpiece, with all eight beamlets of the beam pattern lined up in y-direction. Each beamlet ablates on specific layer (see Figure 3, top left), thus one pass of the scanner movement across the scan field results in the ablation depth equal to eight layers. After each scan line, the scanner moves the beam pattern one scanline along the y-axis (see Figure 3, right).

As shown in Figure 2, the scanner marks a rectangle filled with hatch lines in x-direction. The structure of the bitmap image is created by switching on and off the AOMs, and thus the beamlets at the appropriate positions. The information which pixel is to be ablated in a certain layer is given by the grayscale values of the bitmap. As indicated in section 2.1, the distance between the beamlets on the workpiece is 400 µm. To be able to process bitmaps with arbitrary line distances smaller than 400 µm, the image line closest to the position of each beamlet is chosen in the corresponding layer. For an optimized results, an integer multiple of the line distance should be the distance of the beamlets. If desired, the beamlet distance can be decreased by rotating the orientation of the beam pattern. However, this would require additional data processing to compensate the different x-positions of the beamlets.

The AOMs are switched with a time-based control scheme. The FPGA is connected to the laser trigger signal which indicates the beginning of marking ($t_{trigger}$) for a given scan-line. The mark speed on the workpiece is constant due to the use of the Skywriting function of the scanner (Scanlab AG 2015). Hence, the current laser position in x-direction can be calculated as $pos_x = v_{mark} \cdot (t_{now} - t_{trigger})$ with the mark speed v_{mark}.

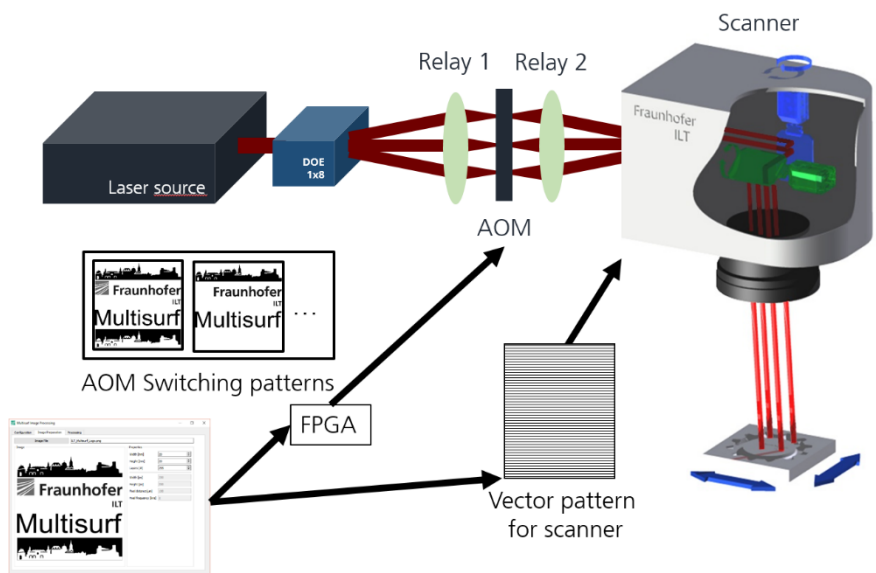

Fig. 2. Experimental setup and control schematics for the multibeam processing. Only three beamlets are shown for clarity. As discussed in Figure 3, the area covered by the scanner needs to be longer than the actual image to be marked in y-direction.

3. Processing

For the purpose of demonstration, the marking of a standardized test structure (see Figure 4) on tool steel is shown. The focus spot diameter on the workpiece is approx. 15 µm. The repetition rate of the laser is set to 400 kHz and the mark speed is set to 4000 mm/s, which corresponds to a pulse to pulse separation of 10 µm on the surface of the workpiece. The same 10 µm are also chosen as the hatch line distance in y-direction. The bitmap has 1000 x 1000 pixel² and covers an area of 10 x 10 mm².

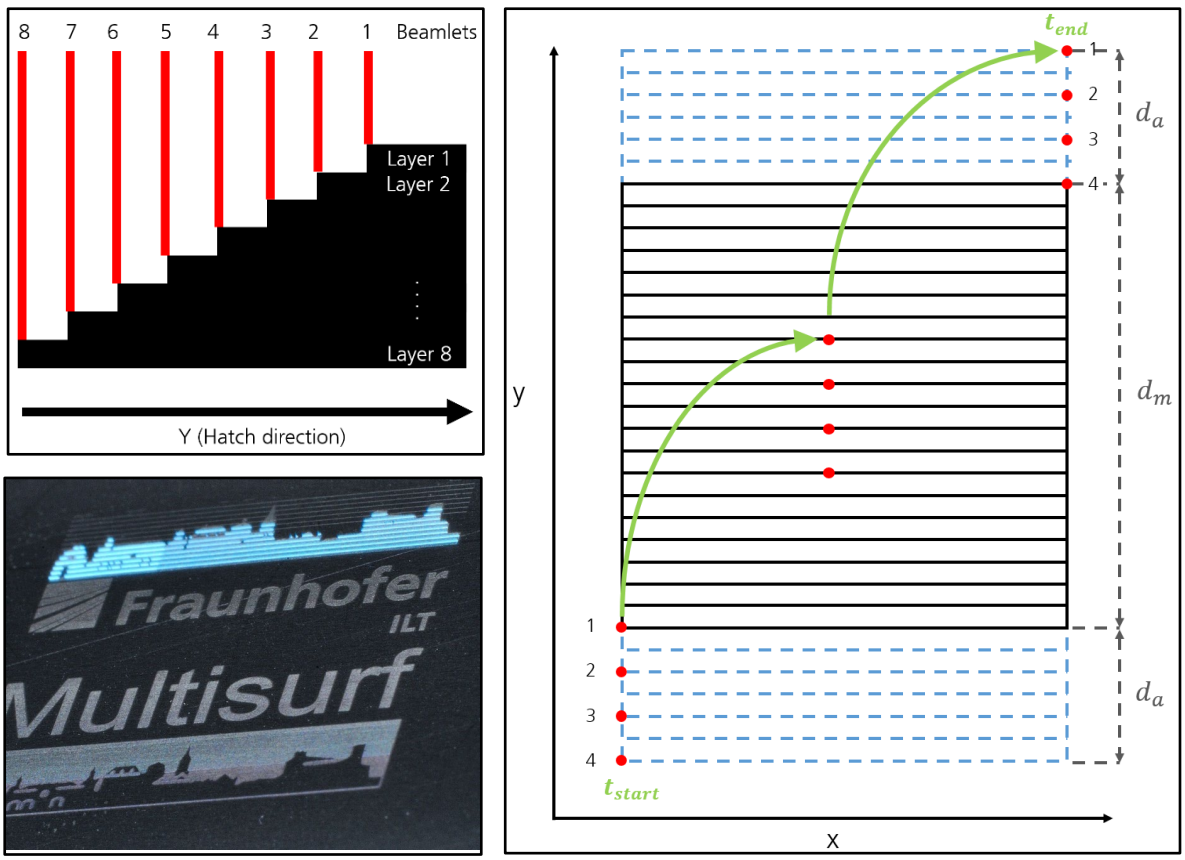

Fig. 3. **Top Left:** Cross section of the workpiece during scanning. Each beamlet processes one certain layer. The scan direction (x) is pointing into the plane of the figure. **Right:** Top view on the workpiece. The black square in the center filled with black solid hatch lines is to be ablated. The green arcs represent the temporal evolution of the position of the beamlets during the process. The beamlets are shown as red dots (only 4 dots are shown for clarity). The scanning of the beamlets starts at t_{start}, and ends at t_{end}. As the last beamlet (4) needs to scan the last hatch line, the effective distance to fill with hatch lines is $d_m + d_a$ with the distance marked d_m and the array width d_a. **Lower Left:** Picture of the ablation process with 8 beams in parallel. Due to the exposure duration of the camera, the beamlets are observed as lines.

As described in section 2.2, only 5.5 W of laser power are available for each beamlet. This is not enough for processing tool steel with pulse bursts of e.g. 5 pulses per burst. Therefore, single pulse processing is used with an average output power of 1.1 W per beamlet. This results in an optimal fluence of 0.8 J/cm² (Neuenschwander et al. 2012). The bitmap is sliced into 256 layers, based on the values of each grayscale pixel. The hatched rectangle (see Figure 2) is scanned 32 times in total, since each pass of the scanner

ablates 8 layers of the bitmap. Figure 3, lower left, shows an image of a running process with the project logo. Here, due to the relatively long exposure time of the camera, the independent beamlets can be observed as eight line scans with different intensity distributions along the scan in x-direction.

Structuring a 10x10 mm² bitmap with 256 layers, a pixel pitch of 10 µm and a mark speed of 4000 mm/s takes 11 minutes with all 8 beamlets. Since the process is bitmap based, this runtime does not vary with the fill grade of the square and does not depend on the particular structure geometry fabricated.

Using a single spot with a bitmap based ablation strategy takes 34 minutes. In direct comparison to the presented multibeam approach, the process time for this general prove of concept is reduced by a factor of 3 already. Pending the optimizations (see Section 6), the runtime will be further reduced and the gain factor will increase to more than a factor of 5, depending on the ablated structure.

4. Results

For evaluation of the processing quality, standardized test structures as shown in Figure 4 are ablated. The resulting structure is of high quality and displays no melt or recast contaminating the surface. Especially, the edges of the circles are free of recast. The reproduction of the fine structures in the circles with feature sizes < 40 µm and the precise, clear cut edges of the circles demonstrate the precise alignment of the 8 beamlets relative to each other and the high precision timing of the AOM switching.

Overall, the quality of the generated microstructures with respect to contour accuracy and feature sizes equal to those of a single spot approach. This includes the ablated depth $d_{ab} \approx 19\mu m$, the general quality of the processing and the resolution of the fine structures.

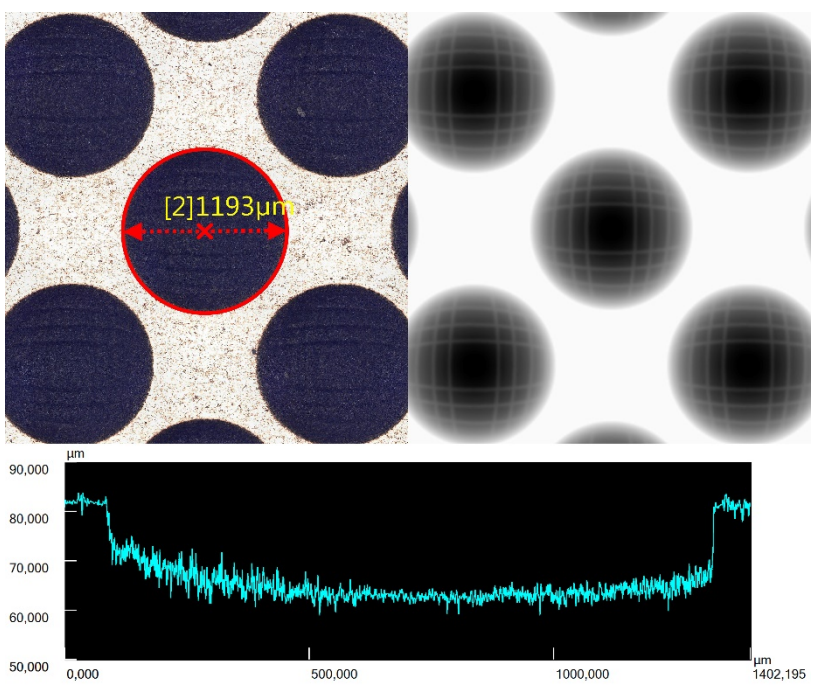

Fig. 4. **Left:** The process result for the ablation of small orbs. **Right:** The bitmap used for the process. **Bottom:** Cross-section of one orb from a Laser-Scanning-Microscope (LSM) measurement. About 19 µm of material are ablated in 256 layers.
The fine structures in the orbs are reproduced accurately, verifying a precise alignment of the 8 beamlets.

5. Conclusion

In this work, we demonstrate a scalable concept for high quality, high precision micro-structuring of arbitrary structures with a switchable multibeam setup. The optics splits the incoming beam into 8 beamlets by means of a DOE, and each beamlet can be switched independently by an AOM during the ablation process. The synchronization between scanner, laser and AOMs is realized by a FPGA and a unified data processing chain approach.

The structuring of a 10x10mm² square on tool steel with 256 layers is demonstrated, with a reduced process duration of just 11 minutes. This represents a threefold improvement compared to a state of the art single beam process. Because the ablation strategy is pixel based on a bitmap image, the reduced process duration is the same for any geometry and fill grade within the square. Potential for further improvement has already been identified and will increase the speed gain to a factor > 5.

The high loss of power due to the sub-70 % efficiency of DOE and AOM is discussed. Only 41 % of the laser power can be applied to the workpiece. Nonetheless, the potential of the approach is shown and the efficiency can be improved by using a higher grade DOE and AOM.

6. Outlook

The process efficiency can be significantly increased even further, for example by optimizing the scanning strategy to only include lines which have to be ablated (see Figure 5). For most geometries, this results in a reduction of processing time between 10 % to 30 %. For some geometries, e.g. a triangle, the improvement will be even bigger.

Furthermore, the concept of switching single beamlets with AOMs is easily scalable. Currently this is the scope of the EU project “MultiFlex” (MultFlex Consortium 2019), which aims to demonstrate an 8x8 beam array with a pitch of 4 mm between neighboring beamlets.

In this work, we were not able to demonstrate burst processing since the effective laser power available in each beamlet was too small. This shortcoming can be addressed with a higher grade DOE and AOM with efficiencies > 80 % and a 150 W laser to reach required fluence of 1.5 J/cm²/pulse in a burst with 5 pulses.

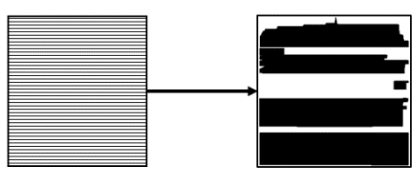

Fig. 5. Optimized scan vectors for the Multisurf-Logo

Acknowledgements

Part of this work has been financed by the German Federal Ministry of Education and Research in the scope of the project “Multisurf”, Grant number 13N13096.

References

AMPHOS GmbH (2019): Products - Amphos. Available online at https://www.amphos.de/products/, checked on 5/3/2019.

Du, Keming; Brüning, Stephan; Gillner, Arnold (2012): High-power picosecond laser with 400W average power for large scale applications. In Friedrich G. Bachmann, Wilhelm Pfleging, Kunihiko Washio, Jun Amako, Willem Hoving, Yongfeng Lu (Eds.): Laser-based Micro- and Nanopackaging and Assembly VI. SPIE LASE. San Francisco, California, USA, Saturday 21 January 2012: SPIE (SPIE Proceedings), 82440P.

Edgewave GmbH (2019): Ultra short pulse lasers | Edgewave. Available online at https://www.edge-wave.de/web/en/produkte/ultra-short-pulse-systeme/, checked on 5/3/2019.

Gillner, Arnold; Jüngst, Michael; Gretzki, Patrick (2015): Multi parallel ultrashort pulse laser processing. In *Lasers in Manufacturing Conference 2015*.

MultFlex Consortium (2019): MultiFlex. Making Ultrafast Lasers Faster. Edited by Fraunhofer Institute for Laser Technology ILT. Available online at https://multiflex-project.eu/, checked on 4/29/2019.

Neuenschwander, Beat; Jaeggi, Beat; Schmid, Marc; Rouffiange, Vincent; Martin, Paul-E. (2012): Optimization of the volume ablation rate for metals at different laser pulse-durations from ps to fs. In Guido Hennig, Xianfan Xu, Bo Gu, Yoshiki Nakata (Eds.): Laser Applications in Microelectronic and Optoelectronic Manufacturing (LAMOM) XVII. SPIE LASE. San Francisco, California, USA, Saturday 21 January 2012: SPIE (SPIE Proceedings), p. 824307.

Raciukaitis, Gediminas (2009): Use of High Repetition Rate and High Power Lasers in Microfabrication: How to Keep the Efficiency High? In *JLMN* 4 (3), pp. 186–191. DOI: 10.2961/jlmn.2009.03.0008.

Russbueldt, P.; Mans, T.; Hoffmann, H. D.; Poprawe, R. (2010): Status quo and outlook of power scaling of ultrafast lasers. In : International Congress on Applications of Lasers & Electro-Optics. ICALEO® 2010: 29th International Congress on Laser Materials Processing, Laser Microprocessing and Nanomanufacturing. Anaheim, California, USA, September 26–30, 2010: Laser Institute of America, pp. 734–740.

Scanlab AG (2015): RTC5 Manual. Puchheim, pp. 124–130.